Correction for Imperfect Camera Motion and Resolution Recovery in Pinhole SPECT

Dirk Bequé, Chris Vanhove, Andriy Andreyev, Johan Nuyts and Michel Defrise.

I. Introduction

Pinhole SPECT is typically applied in small animal imaging, where high spatial resolution is required for imaging small structures in a limited field of view. Care must then be taken not to lose this high resolution information in the subsequent image reconstruction process. We investigate the calibration of a pinhole camera with a slightly oscillating detector tilt and its importance for the quality of reconstructed images. We also investigate the potential for resolution recovery, by modeling the finite dimensions of the pinhole aperture in the reconstruction.

II. Correction for Oscillating Detector Tilt

In [1] we developed a method to determine the acquisition geometry of a pinhole camera, based on the projection centroids of 3 point sources. Like other methods [2], our method assumes a *rigid* camera-collimator assembly that rotates around a *fixed axis* during data acquisition. Seven parameters are then needed to specify the acquisition geometry. The parameters are illustrated in figure 1. For this study, the most important parameters are the focal length f and the distance d, the respective distances from the detector to the focal point and from the detector to the axis of rotation, chosen to be the z-axis. The tilt Φ further indicates the inclination of the detector with respect to this axis of rotation. The four remaining parameters are the electrical shifts e_u and e_v, the mechanical shift m, and the rotation angle Ψ of the detector within the detector plane.

Figure 2(a) shows the centroids of the projections of three point sources measured on a single head DSX camera (SMV), and the estimated centroids which best fit these measurements under the assumption of a rigid detector and fixed rotation axis. A similar measurement was also obtained with an e.cam camera (Siemens). Clearly, the 7 parameter model from [1] results in a significant mismatch between the measured and estimated centroids. This unsuccessful calibration is expected in turn to affect the accuracy of image reconstruction. The most plausible explanation for the failing calibration is that the detector has a slight oscillation around its supporting arm during the rotation of the camera. We found that this oscillation is well modeled by a sinusoidal variation of the tilt angle around an axis inside the crystal and as a function

A. Andreyev, M. Defrise and C. Vanhove are with the Dept. of Nuclear Medicine, V. U. Brussel, B-1090 Brussel, Belgium, D. Bequé and J. Nuyts are with the Dept. of Nuclear Medicine, K.U.Leuven., B-3000 Leuven, Belgium.

Work supported by K.U.Leuven grant OT-00/32, F.W.O. grant G.0174.03, K.U.Leuven grant IDO/02/012 and I.W.T. grant SBO - ANIMONE.

(e-mail: dirk.beque@uz.kuleuven.ac.be)

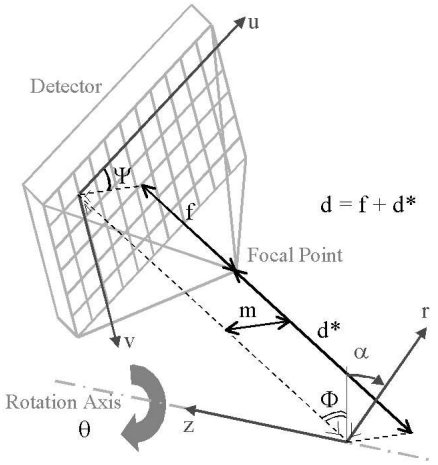

Fig. 1. The parameters describing the pinhole acquisition geometry.

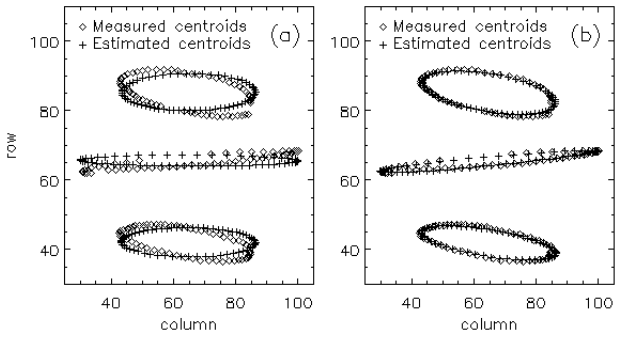

Fig. 2. Measured and estimated centroids of the projections of the 3 calibration point sources, (a) when neglecting the oscillating tilt angle and (b) when incorporating the oscillating tilt angle. The focal length is 201.6 mm and the radius of rotation is 44.1 mm.

of the projection angle θ, yielding $\Phi_\theta = \Phi + \Delta\Phi \cos(\theta + \beta)$. Since the oscillation axis does not intersect the axis of rotation, this model further leads to a variable distance d_θ and variable coordinate z_θ, as can be seen from figure 3. These parameters are computed as $d_\theta = d\cos\Phi/\cos\Phi_\theta$ and $z_\theta = z - (d\sin\Phi - d_\theta \sin\Phi_\theta)$ respectively. With this extended pinhole model, containing two additional parameters $\Delta\Phi$ and β, a much closer match between the measured and estimated centroids is obtained, as shown in figure 2(b).

III. Resolution Recovery

In previous studies with the DSX camera, image reconstruction was done with an implementation of the OSEM algorithm that does not model attenuation, scatter and system

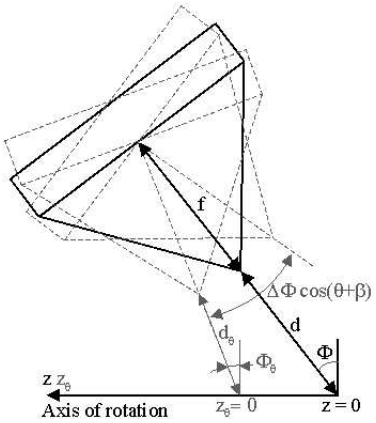

Fig. 3. Model of the oscillating detector tilt.

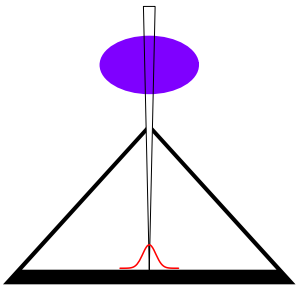

Fig. 4. Pinhole SPECT gamma camera. Collimator blurring and detector response function are shown.

response. The two former effects are expected to have a minor influence for small animal imaging, especially when absolute quantification is not required, for example with gated cardiac studies performed on rats [3]. Modeling the aperture of the pinhole collimator, on the other hand, is important, in particular when large pinhole apertures, up to 3 mm in diameter, are used to improve sensitivity.

Several techniques have been described to model the collimator response within the forward- and back- projectors of an iterative algorithm. When the full transition matrix cannot be kept in memory, the problem is complex, especially with divergent or pinhole collimators and even more when the system geometry is not described by a perfect rotation, as in section II. We have implemented a simple forward-projector similar to the "inverse-cone" method in [4], where each projection pixel is calculated as the weighted average of seven rays, each of which is calculated as a simple line integral of the current image estimate, using the method of Joseph [5]. The seven rays intersect the circular opening of the pinhole in a hexagonal pattern with one of the points at the center, as shown in figure 5(a). We chose the location and the weights of the points according to a standard quadrature method for 2D integration on a disk [6], [7]:

$$\frac{1}{\pi R^2}\int\int_C f(x,y)dxdy = \sum_{i=1}^{n=7} w_i f(x_i,y_i) + O(R^6)$$

where (x,y) is the position of a point in the pinhole aperture, $f(x,y)$ is the value of the line integral linking a fixed detector

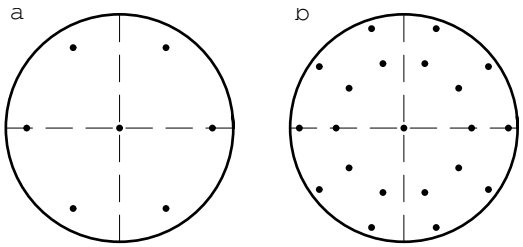

Fig. 5. The 7 and 21 points integration patterns [6].

pixel to the point (x,y) and $C = \{(x,y) : x^2+y^2 \le R^2\}$ is the circular aperture of radius R. The integration points (x_i,y_i) and the corresponding integration weights w_i are listed in Table II.

In addition, we have implemented a method which uses $n = 21$ rays (figure 5(b)), and ensures that all polynomials in (x,y) up to degree 9 are integrated exactly. We use an unmatched voxel driven backprojector, which does not model the pinhole aperture.

In all results shown below, septal penetration [8] was neglected so that an ideal circular aperture was assumed. However, correction for septal penetration may be important when smaller pinhole diameter and/or radiotracers which produce high-energy photons are used (see figure 7). That is why we have developed an improved quadrature method, which takes into account an approximate analytical model of septal penetration for normally incident photons:

$$\frac{1}{\pi R^2}\int\int_{\mathbb{R}^2} f(x,y)a_\mu(\sqrt{x^2+y^2})dxdy \simeq \sum_{i=1}^{n} w_i f(x_i,y_i)$$

where $a_\mu(r)$ is the radial sensitivity function,

$$\begin{aligned} a_\mu(r) &= 1 \quad r \le R \\ &= \exp\left(-2\mu(r-R)\cot\theta\right) \quad r > R \end{aligned}$$

where μ is the linear attenuation coefficient of the gamma rays in lead or tungsten, and θ is the angle of the knife-edge pinhole (see figure 7). Our method uses 7 points and integrates exactly polynomials of degree up to 5. This method still awaits experimental validation.

IV. Results and Discussion

A. Calibration measurements

Four calibration measurements were performed on the DSX camera and the extended calibrations consistently indicated an oscillation of the tilt with amplitude $\Delta\Phi = 0.3^o$ and a phase β ranging from 0.0^o to -0.6^o. Table I lists the results of these calibration measurements.

Only the calibrations with oscillating tilt yield close matches between the estimated and measured point source projections like in figure 3 (b). The reconstructions based on the extended calibration procedure are superior to those obtained when the standard calibration procedure was used. This is illustrated in figure 6 for one of the measurements with the 1.5 mm pinhole aperture. With variable tilt compensation, the reconstructed point sources resemble much closer the expected symmetrical blob-shaped activity distribution than without compensation.

TABLE I

CALIBRATION RESULTS OF THE DSX CALIBRATION MEASUREMENTS. MEASUREMENTS 1 AND 2 WERE PERFORMED WITH THE 1.5 MM PINHOLE APERTURE AND AN IDENTICAL ACQUISITION GEOMETRY. MEASUREMENTS 3 AND 4 WERE PERFORMED WITH THE 3MM PINHOLE APERTURE AND AN IDENTICAL ACQUISITION GEOMETRY.

#	f [mm]	d [mm]	m [mm]	e_u [mm]	e_v [mm]	Φ [deg]	$\Delta\Phi$ [deg]	β [deg]	Ψ [deg]
Without oscillating tilt									
1	198.3	241.8	1.4	-6.0	2.3	2.04	0.00	0.00	-0.34
2	199.8	243.5	0.9	-2.2	-0.6	1.28	0.00	0.00	-0.20
3	193.5	242.3	1.9	-6.6	4.9	2.81	0.00	0.00	-0.58
4	191.2	240.4	1.2	-3.0	5.5	2.91	0.00	0.00	-0.59
With oscillating tilt									
1	200.6	244.7	0.2	0.8	3.2	1.11	0.31	-0.09	-0.19
2	201.6	245.7	0.1	2.3	3.3	1.36	0.31	-0.01	-0.12
3	196.7	246.2	0.1	2.8	4.2	1.45	0.31	-0.63	-0.17
4	195.0	244.1	0.2	2.2	4.9	1.62	0.31	-0.40	-0.19

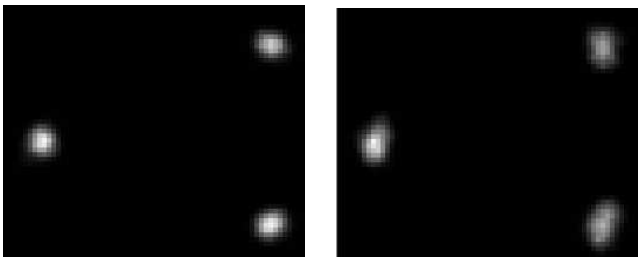

Fig. 6. Reconstructed calibration sources with 1.5 mm pinhole, with (left) and without (right) variable tilt. Reconstruction from 64 128x128 projections. Image was 128x128x128 with 0.5 mm cubic voxels. OSEM with 8 subsets and 4 iterations, without resolution recovery. A longitudinal slice is shown with the vertical axis along the tomographic axis z. Each image is scaled to its own maximum. The distance separating the two sources on the right is 19 mm.

TABLE II

INTEGRATION WEIGHTS FOR 7 RAYS METHOD [5].

Coordinates (x_i, y_i)	Weight w_i
$(0,0)$	$1/4$
$(\pm\sqrt{\frac{2}{3}}R, 0)$	$1/8$
$(\pm\sqrt{\frac{1}{6}}R, \pm\frac{R}{2}\sqrt{2})$	1/8

TABLE III

SIMULATION AND RECONSTRUCTION PARAMETERS.

Pinhole diameter (mm)	1
Focal lenth (mm)	200
Distance between the PH and the axis of rotation (mm)	44
Total number of counts	5000000

Compared to the severity of its effect on image acquisition, the amplitude of the tilt variation is surprisingly small, but at the same time this makes it a plausible explanation of the calibration measurements. So far, we have measured an oscillating detector tilt on two cameras of different manufacturers.

B. Resolution recovery results

In order to understand which kind of improvement we get and how our resolution recovery method works with noisy data we did the following computer simulations. We compared the resolution recovery of our modified OSEM algorithm to OSEM without recovery using simulated noisy projections. Projections were simulated as weighted average of 2500 rays (to model carefully the pinhole aperture) and then convolved with a Gaussian with FWHM of 3.8 mm (to model the intrinsic detector response function of the gamma camera). The results are shown in figure 8. The parameters used for the simulation are listed in Table III.

We reconstructed simulated data using OSEM without any recovery and using OSEM with both the 7 rays Gaussian quadrature method and modeling of the intrinsic response function with a Gaussian kernel.

We estimated the FWHM in the following way: we convolved an ideal sphere of 6 mm diameter with a 3D Gaussian kernel, and determined the parameters of this kernel that optimize the fit with the image of the sphere obtained by reconstructing noiseless data with and without resolution recovery. To study noise amplification we added Poisson noise to our simulated data. Noise is determined as the standard deviation of a ROI in the reconstruction of a simulated uniform sphere of 30 mm diameter. Results show a significant improvement of the compromise between resolution and noise using a 2D Gaussian quadrature method to correct for pinhole blurring and a Gaussian kernel to model the intrinsic detector blurring.

Modeling the pinhole response is all the more important when the aperture is large. Figure 9 illustrates the reconstruction of the three calibration sources, this time measured with a 3 mm pinhole. The improvement of the resolution is significant for this high contrast object, but the effect on noise still has to be analyzed.

One pinhole SPECT bone scan (MDP) of a rat has also been

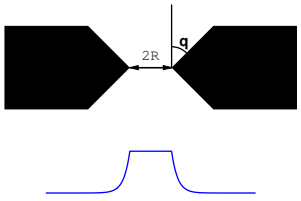

Fig. 7. Collimator pinhole apperture and corresponding circular profile function.

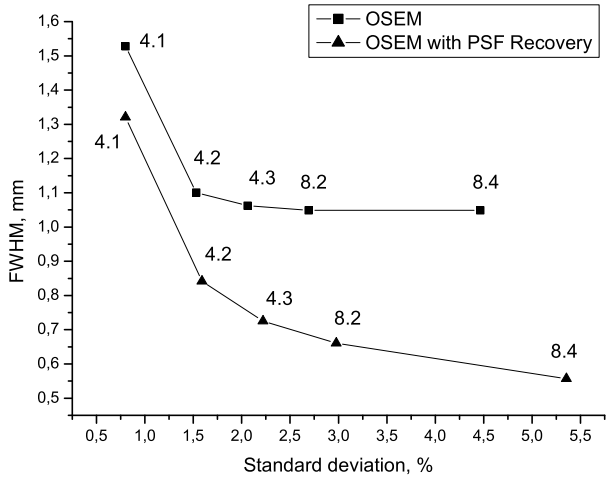

Fig. 8. FWHM vs noise dependency. Reconstructions from 128 128x128 simulated projections. Images are 128x128x128 with 0.33 mm cubic voxels. Numbers near each point correspond to number of subsets and iterations respectively.

processed and here again (figure 10), significant improvement was observed, e.g. in the definition of the ribs.

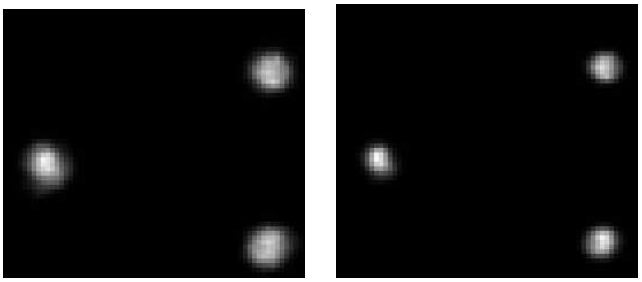

Fig. 9. Reconstructed calibration sources with 3 mm pinhole, without (left) and with (right) response modeling and both with the extended calibration. Reconstruction from 64 64x64 projections. Image is 128x128x128 with 0.5 mm cubic voxels. OSEM with 8 subsets and 4 iterations. Longitudinal slice with each image scaled to its own maximum.

V. Conclusion

Slight variations of the detector tilt during image acquisition have a clear impact on the image acquisition and result in degraded accuracy of the reconstructed images if no correction is made. Modeling the pinhole aperture also significantly improves image quality.

References

[1] D. Bequé *et al.*, "Characterization of Pinhole SPECT Acquisition Geometry, " *IEEE Trans. Med. Imag.*, Vol. 22(5), pp. 599-612, 2003.
[2] F. Noo *et al.*, "Analytic method based on identification of ellipse parameters for scanner calibration in cone-beam tomography, *Phys. Med. Biol.*, Vol. 45,3489-3508, 2000.
[3] C. Vanhove *et al.*, Reproducibility of left ventricular volume and ejection fraction measurements in rat using pinhole gated SPECT, submitted to *J. Nucl. Med.*.
[4] L. Zeng and G. Gullberg, 3D iterative reconstruction algorithms with attenuation and geometric point response correction, *IEEE Trans. Nucl. Sc.*, Vol. 38, 693-702, 1991.

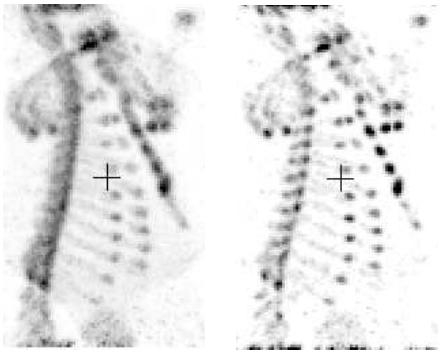

Fig. 10. Reconstructed bone scan of a rat with a 3 mm pinhole, without (left) and with (right) response modeling and both with the extended calibration. Maximum intensity sagittal reprojection. The head is on top, outside the FOV.

[5] TM Joseph "An improved algorithm for reprojecting rays through pixel images". *IEEE Trans. Med. Imag.* vol 1, pp 192-201, 1982.
[6] M. Abramowitz and I. Stegun, Handbook of Mathematical functions, Dover 1972.
[7] JK Brown *et al*, Quantitative SPECT Reconstruction Using Multiray Projection Integrators. Rec. 1995 IEEE MIC Conf., 1272-1276, 1995.
[8] M. Smith and R. Jaszczak, Analytical model of pinhole aperture penetration for 3D SPECT image reconstruction, *Phys. Med. Biol.*, Vol. 43, 761-775, 1998.